ACS APPLIED MATERIALS & INTERFACES

www.acsami.org

Research Article

Curdlan-Decorated Fullerenes Mitigate Immune-Mediated Hepatic Injury for Autoimmune Hepatitis Therapeutics via Reducing Macrophage Infiltration

Chenglong Fei, Lei Liu, Hedong Qi, Yuyang Peng, Jingfen Han,* Chunru Wang, and Xue Li*

Cite This: ACS Appl. Mater. Interfaces 2024, 16, 5536−5547

Read Online

ACCESS | Metrics & More | Article Recommendations | Supporting Information

ABSTRACT: Autoimmune hepatitis (AIH) is a severe immune-mediated inflammatory liver disease whose standard of care is immunosuppressive treatment with inevitable undesired outcomes. Macrophage is acknowledged to aggravate liver damage, providing a promising AIH therapeutic target. Accordingly, in this study, a kind of curdlan-decorated fullerene nanoparticle (Cur-F) is fabricated to alleviate immune-mediated hepatic injury for treating AIH via reducing macrophage infiltration in a concanavalin A (Con A)-induced AIH mouse model. After intravenous administration, Cur-F primarily distributes in liver tissues, efficiently eliminates the excessive reactive oxygen species, significantly attenuates oxidative stress, and subsequently suppresses the nuclear factor kappa-B-gene binding (NF-κB) signal pathway, resulting in the lowered production of pro-inflammatory cytokines and the balancing of the immune homeostasis with the prevention of macrophage infiltration in the liver. The regulation of hepatic inflammation contributes to inhibiting inflammatory cytokines-induced hepatocyte apoptosis, decreasing the serum alanine aminotransferase (ALT) and aspartate aminotransferase (AST) contents and thus ameliorating immune-mediated hepatic injury. Notably, there is no detectable toxicity to the body. Our findings may open up novel avenues for AIH based on curdlan and fullerene materials.

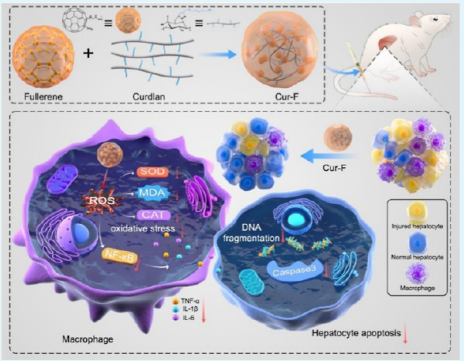

KEYWORDS: *fullerenes, curdlan, autoimmune hepatitis, macrophage infiltration, anti-inflammation*

1. INTRODUCTION

Autoimmune hepatitis (AIH) is a severe immune-mediated inflammatory liver disease that is characterized serologically by the elevated levels of transaminase and autoantibodies and histologically by the destruction of liver parenchyma and interface hepatitis.[1,2] It may cause a rapid failure of liver function like fibrosis, cirrhosis, and hypohepatia, posing enormous threat to human life. The current standard of care for AIH is immunosuppressive treatment, commonly by corticosteroids alone or in combination with azathioprine.[3−5] However, there still exist some adverse outcomes, such as relapse after drug withdrawal, incomplete response, and drug toxicity mainly including cataract, osteoporotic fractures, brittle diabetes, and obesity.[6−8] Therefore, it is an urgent need to develop novel drugs with superior efficacy and lower side-effects for AIH therapeutics.

Although the detailed etiopathogenesis of AIH remains vague, it is acknowledged that the failure of immune homeostasis with a dense infiltrate of immune cells including macrophages in liver plays a central role.[9−11] Activation of macrophages in the liver (mainly Kupffer cells) is reported to produce pro-inflammatory cytokines, leading to the imbalance of the immune microenvironment, the progression of inflammation, and liver damage.[12,13] So, macrophages could be potential targets for AIH treatment.

Fullerene has emerged as a highly powerful platform for disease therapeutics with beneficial biological effects, excellent biocompatibility, and low biotoxicity owing to its pure carbon cage structures and superior reactive oxygen species (ROS) scavenging properties.[14−17] In particular, studies revealed that fullerene or its derivatives alleviated oxidative stress,[18−21] reduced inflammatory response in lung and other tissues,[22−24] protected liver against tetrachloromethane or acetaminophen damage and hepatic steatosis,[25−29] and inhibited overactive immune responses.[30−32] These research studies inspire us to investigate whether fullerene materials play a part in AIH therapeutics.

Importantly, the appropriate decoration of fullerene nanoparticles with specific molecules is decisive for AIH treatment. Curdlan, a linear β-1,3 glucan produced by microorganisms with considerable biocompatibility, bioactivity, and biodegradability,[33] has attracted much attention in drug delivery, anti-

Received: October 29, 2023
Revised: December 23, 2023
Accepted: January 11, 2024
Published: January 24, 2024

Scheme 1. Schematic Illustration of the Preparation and Anti-AIH Mechanisms of Cur-F Nanoparticles

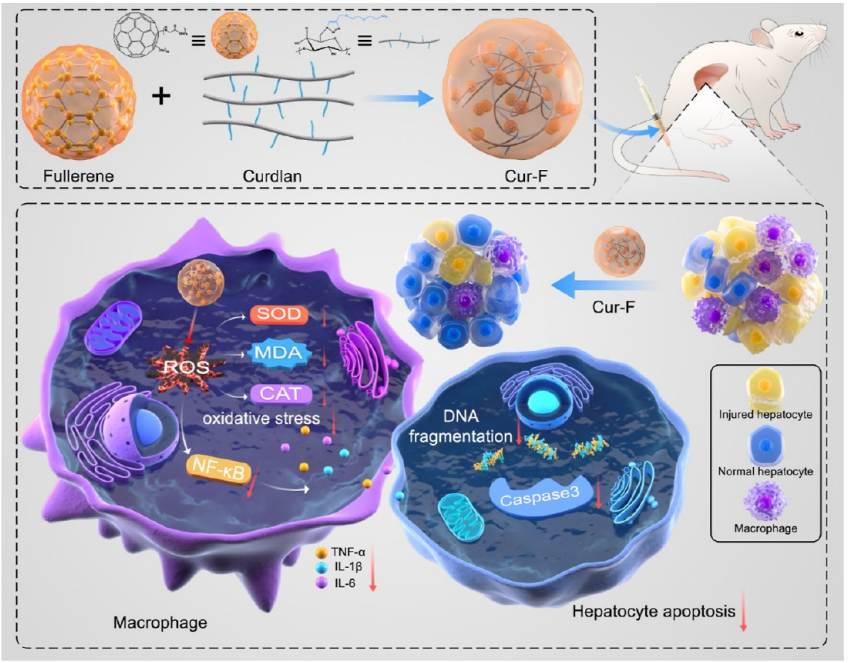

HIV infection, and immunomodulation.[34−37] Numerous studies supported that β-glucan is a pathogen-associated molecule that can be recognized by the dectin-1 receptor expressing on the macrophage, endowing curdlan with macrophage-targeting capability.[38−40]

Therefore, we designed and prepared a curdlan-modified fullerene nanoparticle, defined as Cur-F, for AIH therapeutics via reducing macrophage infiltration (Scheme 1). Cur-F was constructed by a coupling reaction between the carboxylic group on the surface of [60] fullerene and amine groups on curdlan. After intravenous administration, Cur-F primarily accumulated in liver tissues, higher than that of F-Gly. And then, Cur-F eliminated the excessive ROS and alleviated oxidative stress with the equilibrium of oxidoreductase and malonaldehyde (MDA), thereby suppressing the NF-κB signals, reducing pro-inflammatory cytokines levels, and preventing the recruitment of macrophages in liver. Thereby, the alleviation of hepatic inflammation prevented inflammatory cytokines-induced hepatocyte apoptosis and ameliorated immune-mediated hepatic injury. This study provides a promising candidate for AIH therapeutics.

2. MATERIALS AND METHODS

2.1. Materials and Reagents. The C_{60} fullerene was obtained from Fullcan Biotechnology Co. Ltd. Curdlan was obtained from Wako Pure Chemical Industries, Ltd. Ascorbic acid, 1-(3-(dimethylamino)propyl)-3-ethylcarbodiimide hydrochloride (EDC), copper bromide, and *N*,*N*-diisopropylethylamine were purchased from Aladdin. Diglycolamine (DGA), di-*tert*-butyl pyrocarbonate [$(Boc)_2O$], tetrabutyl ammonium hydroxide (TBAH), and 3-bromopropyne were purchased from Innochem. *N*-Hydroxysuccinimide (NHS) was purchased from J&K Scientific. Glycine was purchased from Alfa Aesar. Sulfo-Cy5 amine was purchased from Lumiprobe. Concanavalin A and Hoechst 33342 were purchased from Sigma. 2′,7′-Dichlorodihydro-fluorescein diacetate (DCFH-DA), 2-(4-amidinophenyl)-6-indolecarbamidine dihydrochloride (DAPI), and TUNEL solution were purchased from beyotime. Elisa kits of tumor necrosis factor α (TNF-α), interleukin 1β (IL-1β), and interleukin 6 (IL-6) were purchased from Neobioscience. Elisa kits of superoxide dismutase (SOD), the catalyst (CAT), and MDA were purchased from Nanjing Jiancheng Inc. All reagents and solvents were commercially available and used without further purification.

2.2. Preparation of DGA-Boc. After dissolving DGA (3.36 g) in chloroform (30 mL) and stirring for 0.5 h, a transparent solution was obtained. Then, a solution of $(Boc)_2O$ (6.84 mL) in 30 mL of chloroform was added dropwise in an ice−water bath. The solution was stirred at room temperature for 12 h, forming a faint yellow solution. After washing by water and saturated sodium chloride, drying with anhydrous $NaSO_4$, and evaporating under vacuum, Boc-protected DGA was obtained.

2.3. Preparation of ALK-DGA-Boc. After dissolving DGA-Boc (2.12 g) in anhydrous tetrahydrofuran (100 mL) and stirring for 0.5 h, a transparent solution was obtained. And NaH (0.496 g) was dripped slowly under a nitrogen atmosphere in an ice−water bath for 10 min. Then, a solution of 3-bromopropyne (1.82 g) in anhydrous tetrahydrofuran was added dropwise in an ice−water bath. The solution was stirred at room temperature for 4 h and stopped by adding 6 mL of absolute alcohol. The crude products were separated and purified by silica gel chromatography with *n*-hexane/ethyl acetate (v/v = 4/1).

2.4. Preparation of ALK-DGA. After dissolving ALK-DGA-Boc (5 g) in dichloromethane (DCM, 100 mL) and stirring for 0.5 h, a transparent solution was obtained. Then, trifluoroacetic acid (TFA) in 10 mL of dichloromethane was added slowly to ALK-DGA-Boc and stirred at room temperature for 12 h to remove the *tert*-butyl group. ALK-DGA was obtained after evaporation under vacuum.

2.5. Preparation of Cur-DGA. Cur-DGA was prepared via a click reaction. The solution of Cur-N_3 (0.052 g) dissolved in 5 mL of dimethyl sulfoxide (DMSO) and ALK-DGA (0.2 g) dissolved in 5 mL of DMSO were mixed and stirred for 0.5 h. After that, ascorbic acid (0.06 g), copper bromide (0.032 g), and *N*,*N*-diisopropylethylamine (0.23 mL) were added in order and reacted under a nitrogen atmosphere at room temperature for 3 days. Cur-DGA was obtained after dialysis (3500 Da) and freeze−drying.

2.6. Preparation of F-Gly. Glycine-modified [60] fullerene (F-Gly) was prepared via a liquid−liquid reaction. Solid C_{60} (0.072 g) was dissolved in 60 mL of toluene. Glycine (0.75 g) was dissolved in 8 mL of ultrapure water, and then NaOH (0.79 g) was added. Then, the solutions mentioned above were mixed and vigorously stirred, which reacted for 2 days at 80 °C after adding 5 drops of TBAH (40%). F-Gly was obtained after precipitation and dialysis (3500 Da).

https://doi.org/10.1021/acsami.3c16168
ACS Appl. Mater. Interfaces 2024, 16, 5536−5547

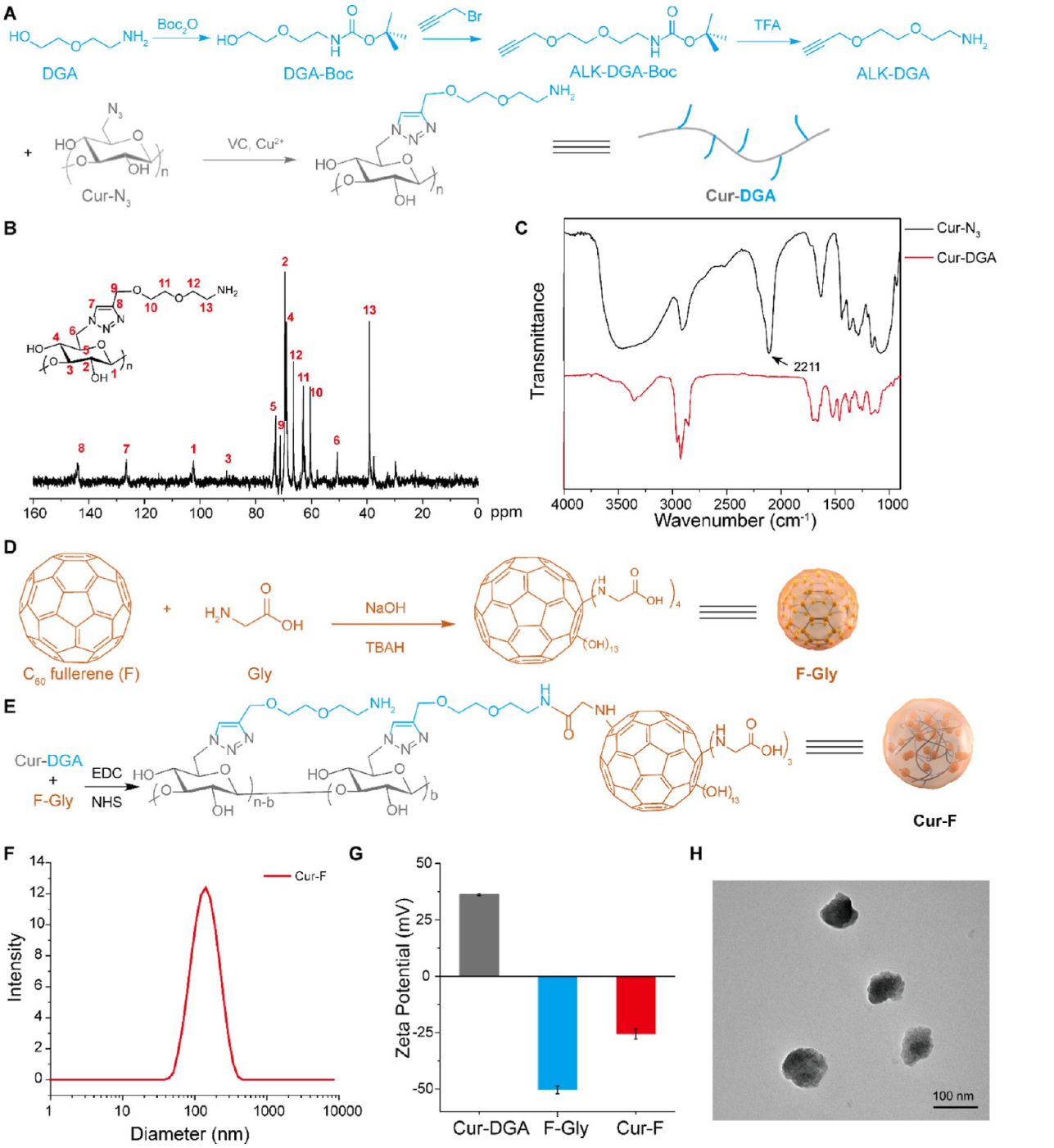

Figure 1. Synthesis and characterization of Cur-F. (A) Illustration of the synthesis of Cur-DGA. (B) ^{13}C NMR spectrum (400 MHz, D_2O, 298 K) of Cur-DGA. (C) FT-IR spectra of Cur-N_3 and Cur-DGA. (D) Illustration of the synthesis of F-Gly. (E) Illustration of the synthesis of Cur-F. (F) Hydrodynamic size of Cur-F analyzed by DLS. (G) Zeta potentials of Cur-DGA, F-Gly, and Cur-F analyzed by DLS. (H) TEM image of Cur-F.

2.7. Preparation of Cur-F. F-Gly (0.062 g) was dissolved in 10 mL of ultrapure water, followed by the addition of EDC (0.076 g) and NHS (0.012 g) and stirring for 1 h. Then, Cur-DGA (0.0108 mg) was added to the above solution for 40 h at room temperature. At last, Cur-DGA was obtained after dialysis and freeze−drying.

2.8. Characterization. The structure of materials was determined by ^1H nuclear magnetic resonance (NMR) and ^{13}C NMR (AVANCE 400, Bruker, Germany) spectroscopy, electrospray ionization mass spectrometry (ESI-MS, Orbitrap Fusion LUMOs, Thermo Fisher Scientific, USA), Fourier transform infrared (FT-IR) spectrometry (Nicolet iN10 MX, Thermo Fisher Scientific, USA), thermogravimetric analysis (TGA, DTG-60 H, Shimadzu, Japan), and elemental analysis (EA, Flash EA 1112, Thermo Fisher Scientific, USA). The particle sizes and Zeta potentials were determined by dynamic light scattering (DLS, Nano-ZS90, Malvern, UK). The particle size was also determined by transmission electron microscopy (TEM, Hitachi HT 7700, Hitachi, Japan) and atomic force microscopy (AFM, NanoWizard 4 NanoScience, JPK, Germany). The ability for scavenging ROS was evaluated by electron paramagnetic resonance (EPR, FA-200, JEOL, Japan). The degree of substitution (DS) of fullerene is calculated by EA of Cur-F according to the following formula: C/N = [13 × (1-DS) + 68DS]/[4 × (1-DS) + 4DS]× 12/14, where C/N represents the weight ratio of C and N elements in Cur-F.

https://doi.org/10.1021/acsami.3c16168
ACS Appl. Mater. Interfaces 2024, 16, 5536−5547

2.9. Labeling of Cur-F with Cy5. EDC (23.7 mg) and NHS (35.7 mg) were added to the Cur-F solution (15 mg of Cur-F dissolved in 10 mL of MES buffer solution) and stirred in the dark for 1 h. Sulfo-Cy5 amine dissolved in PBS was mixed with the above solution and stirred at room temperature in the dark for 2 days. Cur-F-Cy5 was obtained after purification by Sephadex.

2.10. Cell Experiments. L02 and RAW 264.7 cells were obtained from the Institute of Basic Medical Sciences, Chinese Academy of Medical Sciences, China, and cultured in RPMI 1640 and DMEM culture medium supplemented with 10% FBS, 100 μg/mL penicillin, and 100 μg/mL streptomycin in 5% CO_2 at 37 °C in a humidified incubator. To evaluate the cytotoxicity of Cur-F, L02 and RAW 264.7 cells were cultured in 96-well plates for 12 h and treated by Cur-F at different concentrations for 24 h. Cell viabilities were examined by the cell counting kit-8 (cck-8). To evaluate the ability for scavenging ROS, RAW 264.7 cells were seeded in confocal dishes and treated with Cur-F (200 μg/mL) for 4 h and lipopolysaccharide (LPS, 1 μg/mL) for 4 h in order. Then, the cells were incubated with 10 μM DCFH-DA for 30 min and Hoechst 33342 for 3 min. ROS levels in cells were detected by confocal microscopy (FV1000-IX81, Olympus, Japan). To evaluate the antioxidative stress of Cur-F, L02 and RAW 264.7 cells were seeded in 96-well plates for 12 h, treated with Cur-F at different concentrations, and then cultured with H_2O_2 for 1 h. Cell viabilities were examined by cck-8. RAW 264.7 cells were incubated in confocal dishes for 24 h and then were pretreated with 10 μM anti-dectin-1 and anti-TLR2 blocking antibody for 1 h. Then, the fullerene treatment group was incubated with Cur-F-Cy5 for 6 h at 37 °C. Finally, the cells were stained with 5 μg/mL Hoechst 33342 for 10 min, and the fluorescence images were taken by a confocal laser scanning microscope.

2.11. Animal Experiments. BALB/c mice (male, 7 weeks old) were purchased from Beijing Huafukang Bioscience Co. Inc. (Beijing, China). Mice were randomly divided into five groups (6 mice in each group): control, injected with saline (i.v.) and treated with saline (i.v.); Con A, injected with con A (i.v., 15 mg/kg) and treated with saline (i.v.); Cur-DGA, injected with con A (i.v., 15 mg/kg) and treated with Cur-DGA (i.v., 5.74 mg/kg); F-Gly, injected with con A (i.v., 15 mg/kg) and treated with F-Gly (i.v., 14.26 mg/kg); and Cur-F, injected with con A (i.v., 15 mg/kg) and treated with Cur-F (i.v., 20 mg/kg). Drugs for treating AIH were injected intravenously for 3 days once a day. One hour after the last injection, Con A was injected intravenously. And mice were sacrificed 12 h after Con A injection. The liver and spleen were photographed and weighed for the organ index. All the animal studies were approved by the Animal Ethics Committee of Institute of Chemistry, Chinese Academy of Sciences (CAS) (no. 2018-0033).

2.12. Histopathology and Immunofluorescence. The major organs (heart, liver, spleen, lung, and kidney) were collected, fixed in 4% paraformaldehyde, embedded in paraffin, sliced, dewaxed, and rehydrated with a series of gradient concentrations of ethanol. For hematoxylin and eosin (H&E) staining, the sections were stained with hematoxylin and eosin. For TUNEL staining of liver tissues, the sections were incubated with TUNEL solution at 37 °C for 1 h and observed using a digital pathological scanner (KF-PRO-020, KFBIO technology for health, China). For macrophage immunofluorescence imaging of liver tissues, the sections were incubated with the PerCP-Cyanine5.5 labeled F4/80 monoclonal antibody (58-4801-82, Thermo Fisher Scientific, USA) and DAPI and observed by confocal microscopy (FV1000-IX81, Olympus, Japan). The quantitative analysis was carried out using Image J software.

2.13. Biochemical Analysis. The levels of alanine aminotransferase (ALT) and aspartate aminotransferase (AST) in serum were examined by an automatic biochemical analyzer (TBA-2000FR, Toshiba, Japan). The pro-inflammatory cytokines of TNF-α, IL-1β, and IL-6, the level of ROS in liver tissues, and the redox status-related parameters of SOD, CAT, and MDA were tested by Elisa according to the instructions.

2.14. Quantitative Real-Time Polymerase Chain Reaction. Total RNA was extracted from the liver tissues using Trizol (Invitrogen Life Technologies, USA) according to the instructions. 1.0 μg of total RNA was reverse-transcribed to cDNA using first Strand cDNA synthesis SuperMix (NovoScript, China). Real-time polymerase chain reaction (PCR) analysis for *TNF-α*, *IL-1β*, *IL-6*, and *NF-κB* was performed on a CFX 96 Real-Time system (Bio-Rad, USA) with 2× Novostart SYBR qRT-PCR SuperMixPlus (Novoprotein, China). The primers are listed in Table S1.

2.15. Western Blot. Liver tissues were homogenized in RIPA lysis buffer with protease and phosphatase inhibitors. Proteins were collected after centrifugation at 4 °C at 12,000 rpm for 15 min and heated at 100 °C for 5 min with loading buffer. Then, protein was separated on a 10% gradient SDS-PAGE gel, electro-transferred onto 0.45 μm PVDF membranes, and blocked with 5% skimmed milk powder. The membrane was incubated with the primary antibodies against NF-κB (8242, CST, USA), Bax (ab182733, Abcam, UK), Bcl-2 (3498, CST, USA), caspase3 (ab44076, Abcam, UK), and β-actin (3700, CST, USA) overnight at 4 °C and exposed to the secondary antibody (A0208, Beyotime, China). Chemiluminescence was detected and analyzed with Amersham Imager (AI680, GE, USA) to generate densitometry data.

2.16. Ex Vivo Fluorescence Imaging. The biodistributions of Cur-F and F-Gly were evaluated by fluorescence imaging using the IVIS Spectrum system (PerkinElmer, USA). Cur-F-Cy5 or F-Gly-Cy5 were injected intravenously. At predetermined time intervals (1, 2, 8, 24 h, and 3 d), mice were sacrificed, and the major organs (heart, liver, spleen, lung, and kidneys) were collected and imaged. The fluorescence intensities of the organs were quantified.

2.17. Statistical Analysis. All data are presented as the mean ± standard deviation (SD). Statistical analysis was performed using one-way analysis of variance (ANOVA, IBM SPSS Statistics 25 software). * represents $P < 0.05$ and ** represents $P < 0.01$, analyzed by ANOVA with LSD or Games−Howell tests.

3. RESULTS AND DISCUSSION

3.1. Preparation and Characterization of Cur-F. To facilitate the successful coupling of curdlan and C_{60} fullerene, DGA was first linked to curdlan by a click reaction (Figure 1A). In brief, the amino group on DGA was protected by Boc_2O (DGA-Boc for short), and alkyne was introduced to form ALK-DGA-Boc. Then, ALK-DGA was obtained after removing the Boc group using TFA. The chemical structures of DGA-Boc, ALK-DGA-Boc, and ALK-DGA were confirmed by ^{1}H NMR and ^{13}C NMR spectra with corresponding peaks (Figures S1−S3). And the appearance of peaks at 228.12 [M + Na^+], 266.14 [M + Na^+], and 144.10 [M + H^+] in the ESI-MS spectrum suggested the successful preparation of these molecules (Figures S4−S6). At last, the click reaction was performed between the azide group of curdlan and the alkynyl group of ALK-DGA to form Cur-DGA, whose chemical structure was confirmed by the ^{13}C NMR spectrum (Figure 1B). And the disappearance of the peak at 2111 cm^{-1} in the FT-IR spectrum (Figure 1C), which was ascribed to the N_3 group, also indicated the complete click reaction. The involvement of smart DGA linkers could promote the coupling reaction of curdlan and C_{60}, minimizing the steric hindrance between the main chain of curdlan and carbon cages.

To introduce the carboxyl group on the surface of carbon cages, fullerene was modified by glycine (Gly) via nucleophilic attack of amino groups on Gly under alkaline conditions.[28] After purification and freeze−drying, the structure of F-Gly was characterized by FT-IR spectroscopy, TGA, and EA. As shown in Figure S7, the prominent peaks located at 1604 cm^{-1} (C═C) and 1396 cm^{-1} (C−C) were assigned to C_{60} carbon cages. And the stretching vibration bands of 3400 cm^{-1} (O−H/N−H), 2966 cm^{-1} (C−H), 1720 cm^{-1} (C═O), and 1076 cm^{-1} (C−O/C−N) were ascribed to glycine and hydroxyl groups of F-Gly. The weight loss before 158 °C was about 8.2

https://doi.org/10.1021/acsami.3c16168
ACS Appl. Mater. Interfaces 2024, 16, 5536−5547

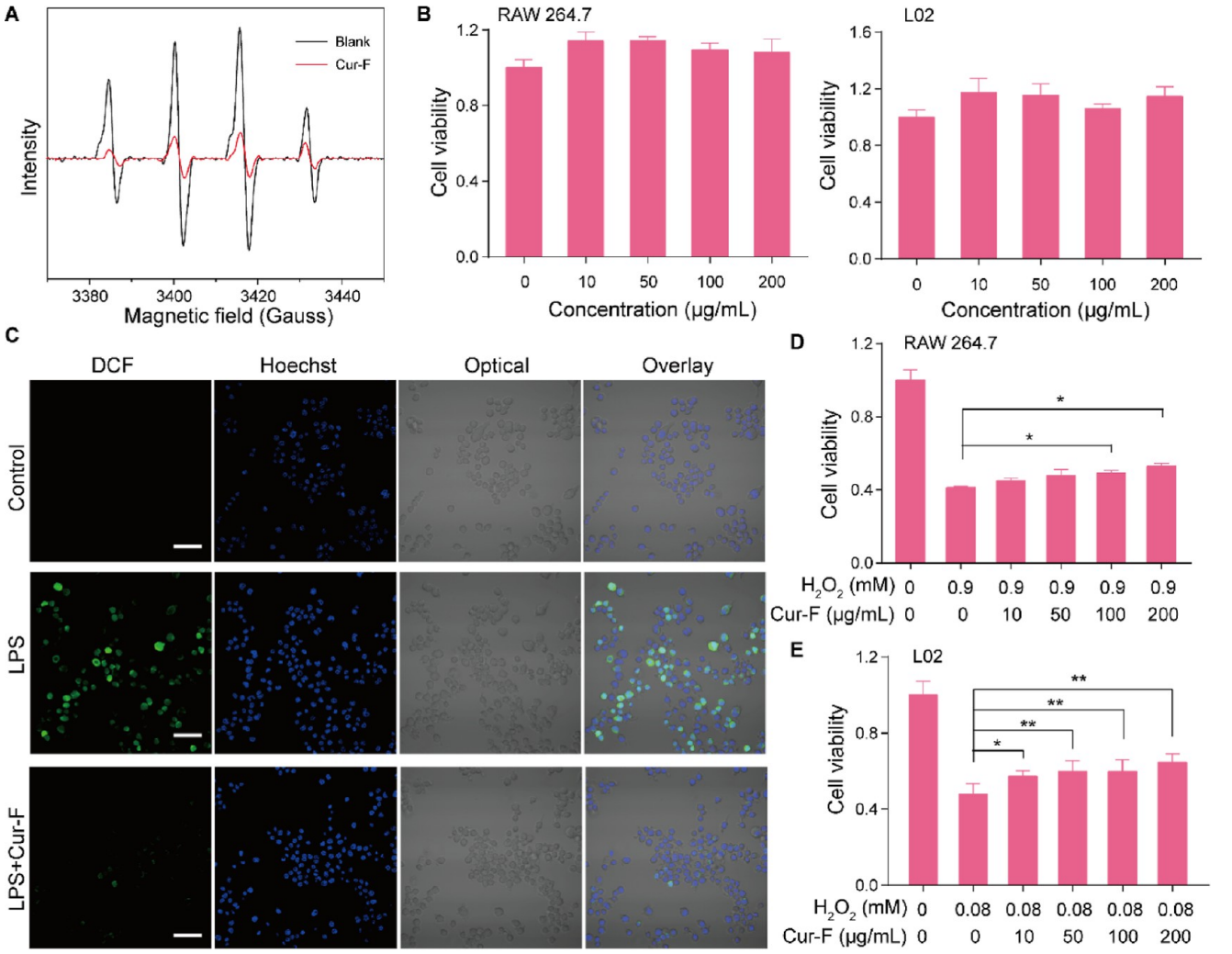

Figure 2. Cur-F scavenges the excessive ROS and protects cells against oxidative damage. (A) EPR analysis of Cur-F. (B) Cell viability of RAW 264.7 and L02 cells after incubation with Cur-F at different concentrations. (C) Confocal images of RAW 264.7 cells stained by DCFH-DA and Hoechst 33342 in control, LPS, and LPS + Cur-F groups. The scale bar is 50 μm. (D,E) Cell viabilities of RAW 264.7 (D) and L02 (E) cells incubated by Cur-F at different concentrations after being injured by H_2O_2. * represents $P < 0.05$ and ** represents $P < 0.01$, analyzed by ANOVA with LSD or Games−Howell tests.

wt % (wt %), which belonged to the bound water of F-Gly (Figure S8A). Additionally, the contents of C, H, and N elements in F-Gly were 60.04, 3.03, and 4.31 wt %, respectively (Figure S8B), delineating that there were ca. 4 glycine groups on each carbon cage. So, the average structure formula of F-Gly was deduced to be $C_{60}(NHCH_2COOH)_{\sim 4}(OH)_{\sim 13}\cdot 6H_2O$.

Lastly, Cur-F was produced by the amidation reaction between Cur-DGA and F-Gly, as illustrated in Figure 1E. The ratio of C (49.15 wt %) and N (6.53 wt %) in EA (Figure S8B) suggested that the DS of F-Gly conjugated on curdlan was 0.6730 (b/n in Figure 1E). Then, the size distribution and zeta potential of nanoparticles were investigated by DLS. The hydrodynamic diameters of Cur-DGA and F-Gly were 657.8 ± 45.1 nm and 132.1 ± 10.5 nm, respectively (Figure S9). After forming Cur-F, the size distribution turned to approximately 149.5 ± 6.8 nm (Figure 1F). The zeta potential of Cur-DGA was 36.3 mV, and the introduction of F-Gly (about −50.3 mV) resulted in a zeta potential of −25.6 mV, suggesting the formation of Cur-F (Figure 1G). The negative charge on the surface of Cur-F made it more favorable for blood circulation. Additionally, the size of Cur-F was also investigated by TEM (Figure 1H) and AFM (Figure S10), demonstrating that Cur-F was with a measured average diameter of ∼78 nm.

3.2. Cur-F Scavenges ROS to Protect Cells against Oxidative Damage. Due to the extended bond system with high electron affinity of carbon cages, the fullerene exhibits excellent antioxidative properties to eliminate free radicals via catalyzing free radicals to new stable substances.[41] To evaluate whether the modification of F-Gly by curdlan impairs its ability to scavenge ROS, we investigated the capability of Cur-F to quench the hydroxyl radical (•OH), a critical ROS component in the physiological and pathological conditions, by EPR. As shown in Figure 2A, Cur-F at the concentration of 80 μg/mL could eliminate about 79.8% of the generated •OH compared with the blank control, which is equivalent to that of F-Gly at the same fullerene concentration (Figure S11), thereby suggesting the retention of the outstanding ROS scavenging capability of Cur-F. Furthermore, we investigated the intracellular antioxidative effects of Cur-F. First, the cytotoxicity of Cur-F was evaluated by coincubation with RAW 264.7 cells and L02 hepatocytes at different concentrations for 24 h. It was

https://doi.org/10.1021/acsami.3c16168
ACS Appl. Mater. Interfaces 2024, 16, 5536−5547

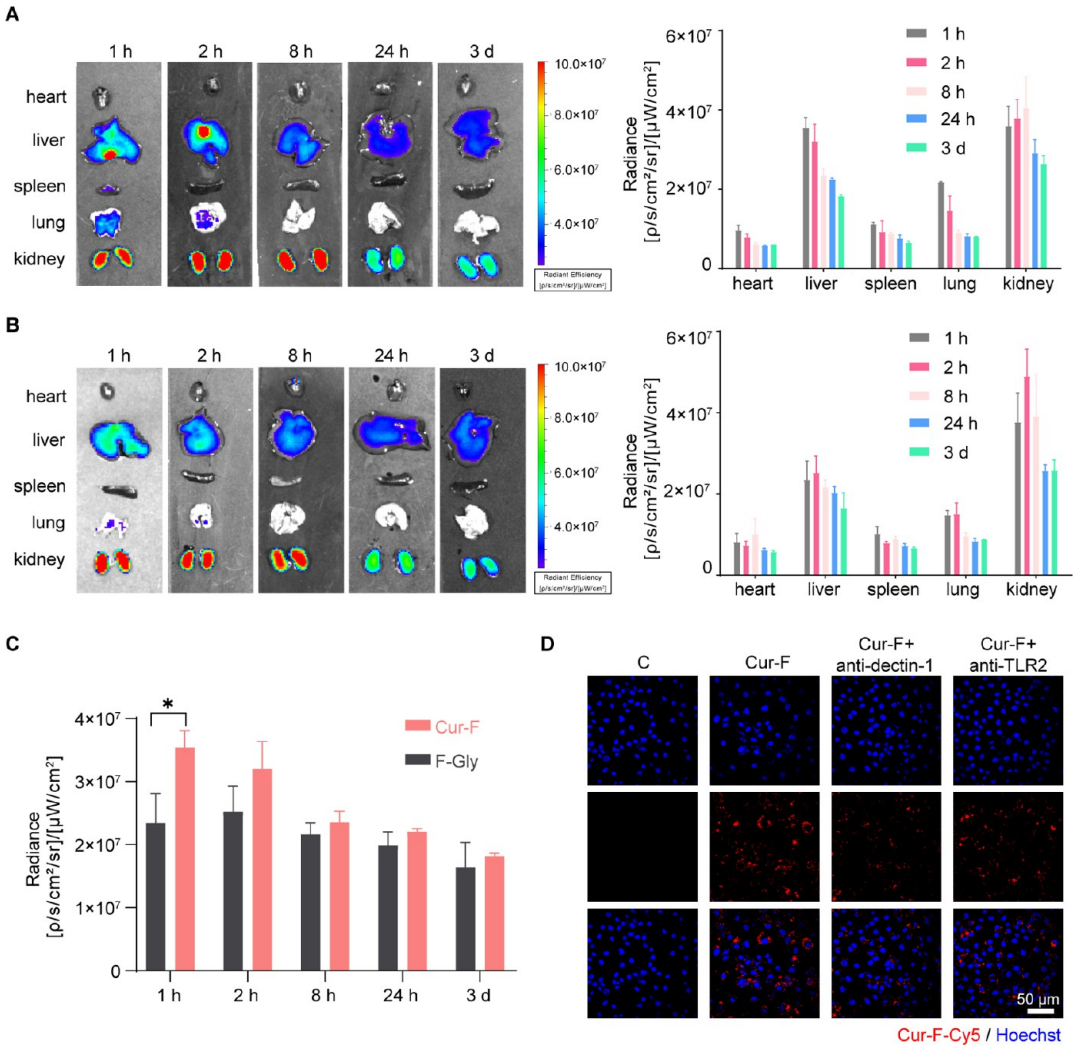

Figure 3. Biodistribution of Cur-F and F-Gly. (A) *Ex vivo* fluorescence imaging of the heart, liver, spleen, lung, and kidney and quantification of the fluorescence intensity after injection of Cur-F-Cy5. (A) *Ex vivo* fluorescence imaging of the heart, liver, spleen, lung, and kidney and quantification of the fluorescence intensity after injection of F-Gly-Cy5. (C) Biodistribution of Cur-F and F-Gly in the liver. (D) Uptake of Cur-F-Cy5 by RAW 264.7 cells. The scale bar is 50 μm.

demonstrated that there was no significant reduction of cell viabilities in Cur-F-treated RAW 264.7 and L02 cells up to the concentration of 200 μg/mL (Figure 2B). On this basis, we explored whether Cur-F eliminated ROS inside cells by DCFH-DA staining. As shown in Figure 2C, lipopolysaccharide (LPS) treatment remarkably increased the intracellular ROS levels of RAW 264.7 cells, which were effectively decreased after treatment by Cur-F. It revealed that the capability of Cur-F to scavenge ROS was not deprived by the complex microenvironment inside cells. Accordingly, Cur-F could significantly protect RAW 264.7 and L02 cells against H_2O_2-induced oxidative damage (Figure 2D,E). All these data depicted that Cur-F efficiently eliminated superabundant ROS and protected cells against oxidative damage.

3.3. Cur-F Primarily Accumulates in Macrophages of Liver Tissues. To explore the biodistribution of Cur-F, we labeled Cur-F with fluorescent Cy5 for fluorescence imaging *via* amidation. BALB/c mice were treated with Cy5-labeled Cur-F (Cur-F-Cy5) or Cy5-labeled F-Gly (F-Gly-Cy5) via tail intravenous injection, and their primary organs (heart, liver, spleen, lung, and kidneys) were harvested for imaging *ex vivo* at different time intervals. It was demonstrated that Cur-F-Cy5 and F-Gly-Cy5 were mainly distributed in liver and kidney tissues (Figure 3A,B), which is consistent with other fullerene-based materials.[42,43] And the distribution of Cur-F in the liver is significantly higher than that of F-Gly (Figure 3C), suggesting the liver-targeting effect of Cur-F. These most abundant Cur-F concentrations in the liver inspired the application of it on hepatic diseases. Then, we investigated the macrophage-targeting ability of Cur-F *in vitro*. The strong red fluorescence signals in the Cur-F group revealed that Cur-F nanoparticles were largely absorbed by RAW 264.7 cells. However, after being blocked by the antibody of dectin-1 and TLR2 (receptors on the macrophage membrane surface that could recognize curdlan), the RAW 264.7 cells exhibited reduced red fluorescence, suggesting that Cur-F can actively target the macrophage and be engulfed by dectin-1- and TLR2-mediated macrophage endocytosis (Figure 3D).

3.4. Cur-F Alleviates Immune-Mediated Hepatic Injury and Inflammation in a Con A-Induced Murine Model of AIH. Considering the above-mentioned accumulation of Cur-F in liver tissues, we explored whether Cur-F alleviates immune-mediated hepatic injury using a mouse AIH model induced by intravenous injection of lectin Con A

https://doi.org/10.1021/acsami.3c16168
ACS Appl. Mater. Interfaces 2024, 16, 5536−5547

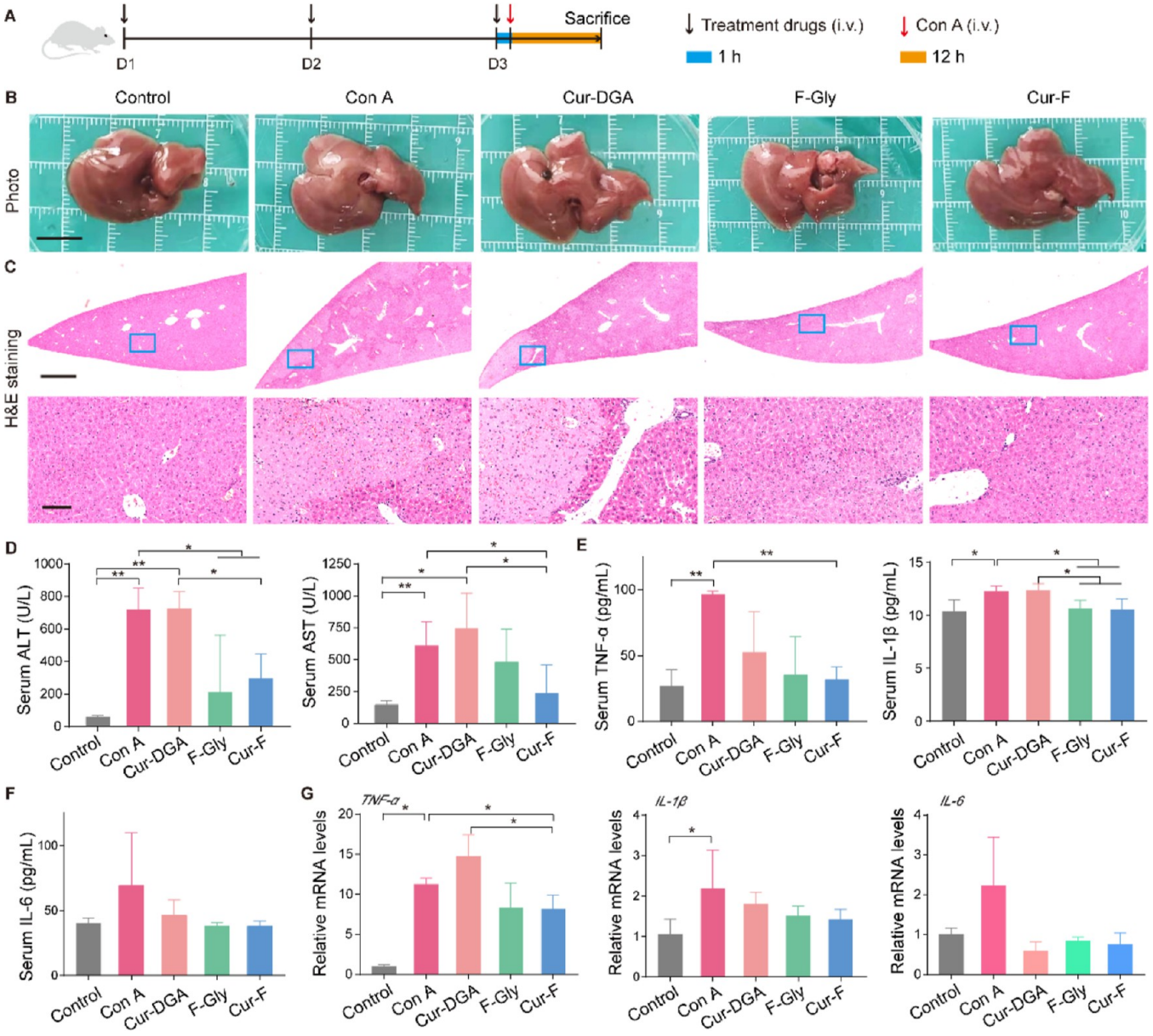

Figure 4. Cur-F alleviates hepatic injury and inflammation induced by Con A. (A) Schematic of the experimental design. (B) Macroscopic appearance of livers. The scale bar is 1 cm. (C) H&E staining of liver tissues in different groups. The scale bar is 1 mm and 100 μm from the top to bottom. (D) ALT and AST analysis. (E,F) Levels of representative inflammatory factors TNF-α, IL-1β, and IL-6 in serum. (G) Relative mRNA expressions of inflammatory factors *TNF-α*, *IL-1β*, and *IL-6* in liver tissues. Data are the mean ± SD n = 3−6 in each group. * represents $P < 0.05$ and ** represents $P < 0.01$, analyzed by ANOVA with LSD or Games−Howell tests.

(Figure 4A), which is a generally accepted experimental model for AIH resembling pathogenesis mechanisms and pathological changes of patients.[44] First, the morphology of the liver was observed. Macroscopically, there were abnormalities in liver organs with a pale and coarse surface in Con A-treated mice, which were reversed by Cur-F (Figure 4B). The liver index exhibited no obvious changes (Figure S12), possibly resulting from the fact that the damage was acute and failed to cause the changes of liver weight. Further, the pathological damages analyzed by H&E staining including the loss of the liver architecture, large-area hepatocyte necrosis, immune cell infiltration, and erythrocyte diapedesis induced by Con A were also remarkably ameliorated by Cur-F (Figure 4C). ALT and AST, the major hepatic enzymes reflecting hepatic functions, were significantly decreased in the serum of Cur-F-treated mice, instead of increases induced by Con A (Figure 4D). In addition, we investigated the effects of Cur-F on inflammatory responses. The levels of representative pro-inflammatory cytokines of TNF-α, IL-1β, and IL-6 were detected in serum, depicting that Cur-F significantly lowered TNF-α and IL-1β levels and reduced IL-6 levels to some extent (Figure 4E,F). And the reduction of mRNA expressions of *TNF-α*, *IL-1β*, and *IL-6* in liver tissues also demonstrated that Cur-F attenuated hepatic inflammation (Figure 4G). However, curdlan alone showed no alleviation for hepatic lesion, and F-Gly alone also improved hepatic disruption and inflammation but was less effective than Cur-F. All these data suggested the excellent anti-AIH effects of Cur-F with hepatoprotection and anti-inflammation.

https://doi.org/10.1021/acsami.3c16168
ACS Appl. Mater. Interfaces 2024, 16, 5536−5547

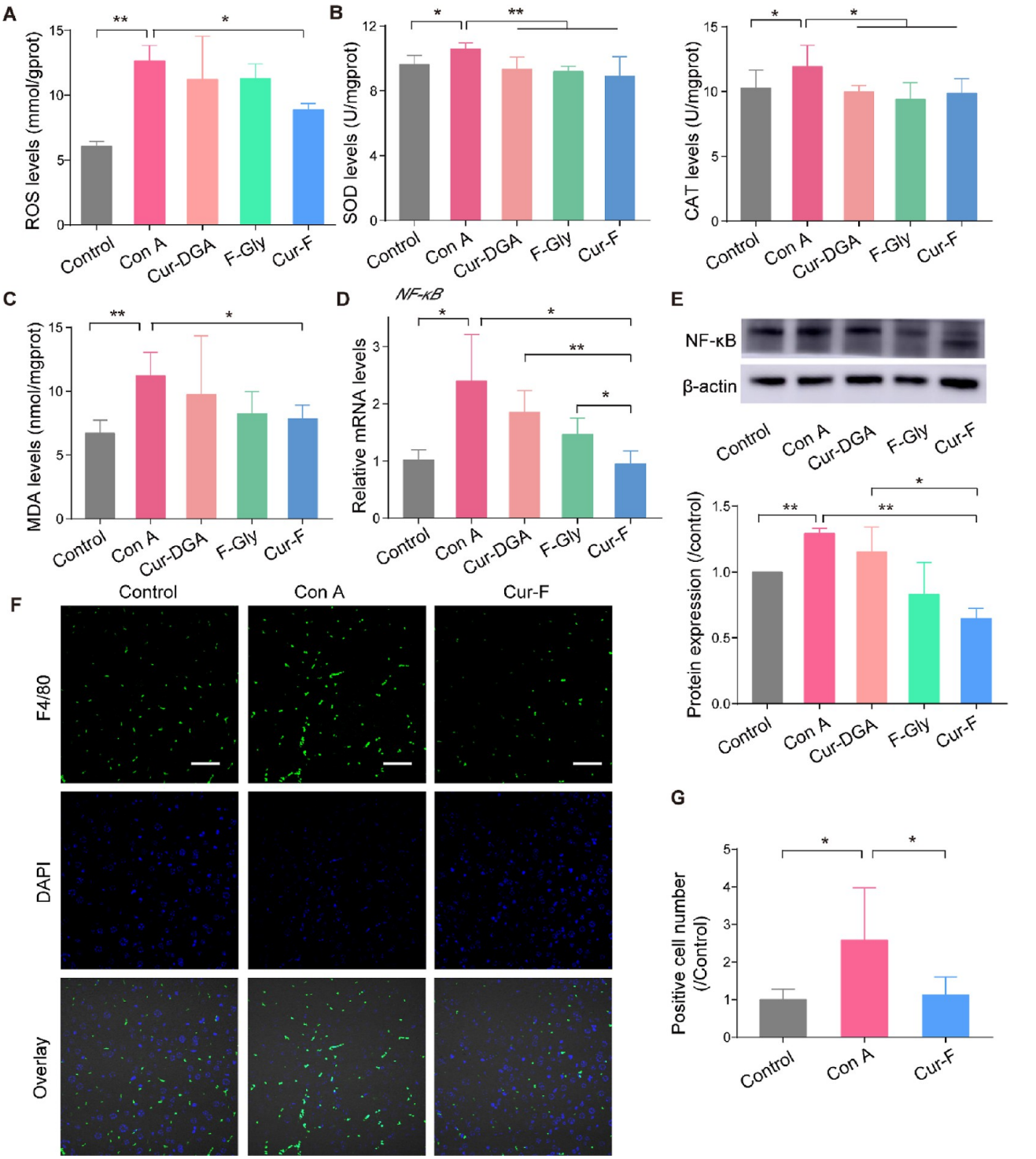

Figure 5. Cur-F protects hepatocytes against oxidative stress and macrophage infiltration. (A) Level of ROS in liver tissues. (B) SOD and CAT levels in liver tissues. (C) MDA levels in liver tissues. (D) Relative mRNA expressions of *NF-κB* in liver tissues. (E) WB and quantitative analyses of NF-κB. (F) Fluorescence microscopy of F4/80$^+$ (green) microphages and DAPI (blue) in liver tissues. The scale bar is 100 μm. (G) Quantitative analysis of immunofluorescence of F4/80. Data are the mean ± SD n = 3−6 in each group. * represents $P < 0.05$ and ** represents $P < 0.01$, analyzed by ANOVA with LSD or Games−Howell tests.

3.5. Cur-F Improves Oxidative Stress and Suppresses Macrophage Infiltration. To further uncover the anti-AIH mechanisms of Cur-F, we first investigated the redox status in liver tissues by detecting the levels of ROS, the typical oxidoreductases of SOD and the CAT, and the product of lipid peroxidation of MDA. It was demonstrated that Con A disturbed the hepatic redox equilibrium with increased SOD and CAT levels in liver tissues to eliminate the excessive ROS (Figure 5A,B). Cur-F scavenged these redundant ROS, significantly decreasing the levels of SOD and CAT and balancing the redox states. In addition, Cur-F reduced the MDA level in liver tissues, which was elevated due to oxidative

https://doi.org/10.1021/acsami.3c16168
ACS Appl. Mater. Interfaces 2024, 16, 5536−5547

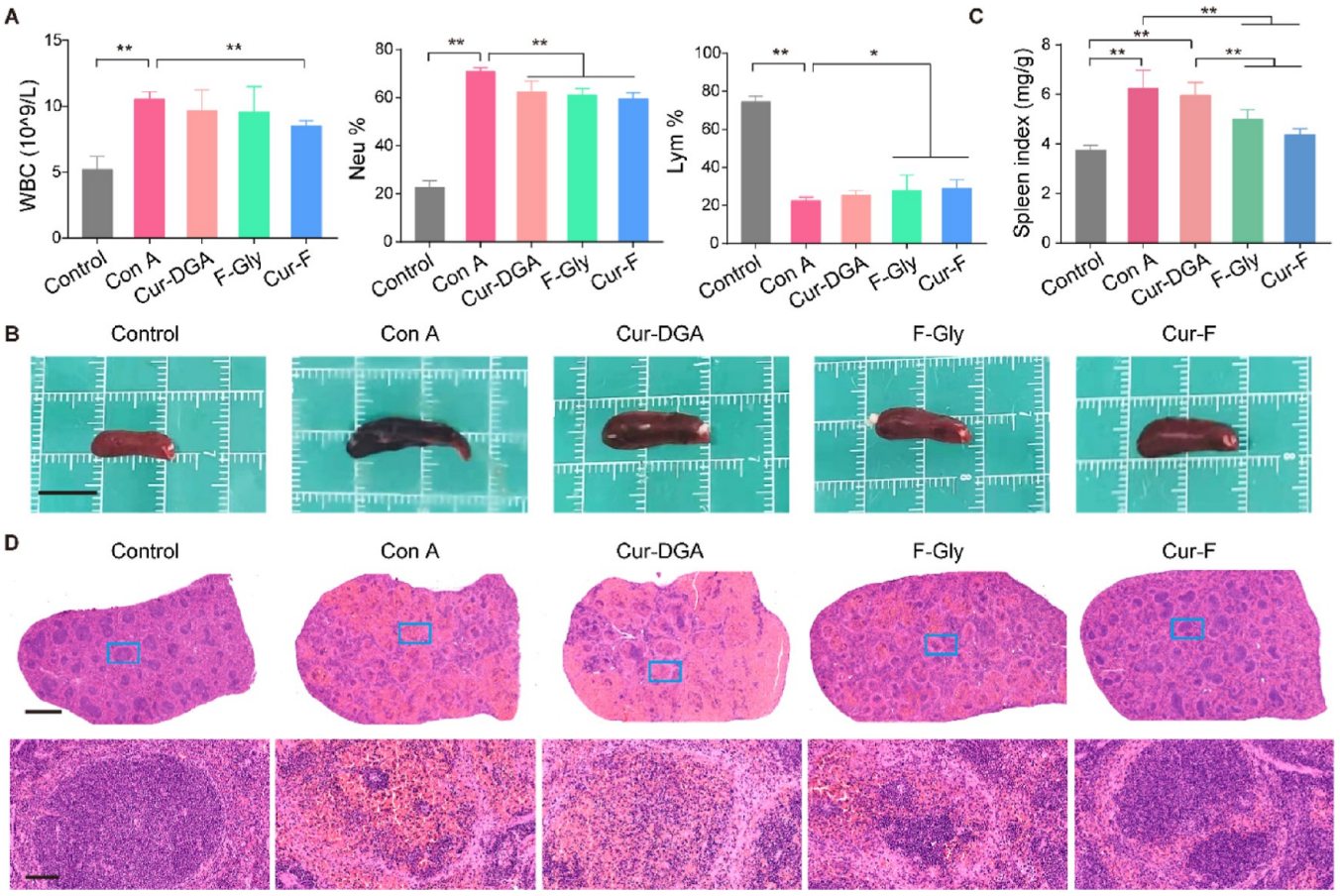

Figure 6. Cur-F improves immune disorders. (A) Contents of WBC, neutrophils, and lymphocytes detected by a routine blood test. (B) Macroscopic appearance of the spleen in different groups. The scale bar is 1 cm. (C) Spleen index. (D) H&E staining of the spleen in different groups. Scale bars are 1 mm and 100 μm from the top to bottom. Data are the mean ± SD n = 3−6 in each group. * represents $P < 0.05$ and ** represents $P < 0.01$, analyzed by ANOVA with LSD or Games−Howell tests.

stress induced by Con A (Figure 5C). It is reported that NF-κB, a family of transcription factors, regulates the expression of various proinflammatory genes and serves as the critical mediator for inflammatory response, which can be activated by ROS.[45,46] Here, we demonstrated that Cur-F significantly reduced both the mRNA levels of *NF-κB* and the protein expression of NF-κB (Figure 5D,E). Macrophages play a crucial role in the pathophysiology of AIH, and the recruitment of macrophages will aggravate the hepatic inflammation. Therefore, the macrophage infiltration in liver was investigated by fluorescence staining of F4/80, manifesting that Cur-F reduced the F4/80 positive cell numbers (Figure 5F,G). All these data indicated that Cur-F alleviated oxidative stress of Con A-induced AIH mice, inhibited the expression of the NF-κB signal molecule, and ameliorated inflammation-induced macrophage infiltration.

3.6. Cur-F Positively Regulates Immune Dysfunction for AIH Therapeutics. Although the exact mechanisms of AIH have not been fully clarified, dysfunction of immune regulation probably plays a critical role.[1] So, we explore the regulation of Cur-F on immune functions. It was demonstrated that Con A increased WBC levels with elevated neutrophils and lowered lymphocytes, suggesting the presence of inflammation and immune dysfunction in AIH mice. Excitingly, Cur-F decreased WBC levels and neutrophil contents and increased lymphocyte contents, alleviating these immune cell disorders (Figure 6A). Spleen is the largest secondary lymphoid organ in the body and hosts a wide range of immunologic functions.[47] Here, spleen was also analyzed under morphological and pathological observation. We found that the spleen of Con A-treated mice was dark, swollen, and irregularly shaped with uneven margins, which was improved by Cur-F (Figure 6B). And Cur-F remarkably reduced the spleen index, instead of it being significantly increased in Con A-treated mice (Figure 6C). The normal spleen tissue was firm and regular in texture with white and red pulp.[48] However, Con A injection distorted the spleen architecture with clearly disordered pulp nodules, loose parenchyma, and massive erythrocyte diapedesis, which was also reversed in mice with Cur-F treatment.

3.7. Cur-F Reduces Hepatic Apoptosis. The hepatic apoptosis was assessed by the terminal deoxynucleotidyl transferase dUTP nick end-labeling (TUNEL) assay and WB. Compared to liver tissues with massive DNA fragmentation (green fluorescence) disrupted by Con A, Cur-F significantly decreased the apoptotic cell numbers (Figures 7A,B and S13). Then, the dominant apoptotic signal pathway of B-cell lymphoma/leukemia 2 (Bcl-2)/Bcl-2 associated X (Bax)/caspase-3[49] was detected (Figure 7C−F). It was demonstrated that Cur-F remarkably decreased the protein expression of Bax, increased the ratio of Bcl-2/Bax, and lowered the protein expression of caspase3 in liver tissues of Con A-induced AIH mice, describing the antiapoptotic effects

https://doi.org/10.1021/acsami.3c16168
ACS Appl. Mater. Interfaces 2024, 16, 5536−5547

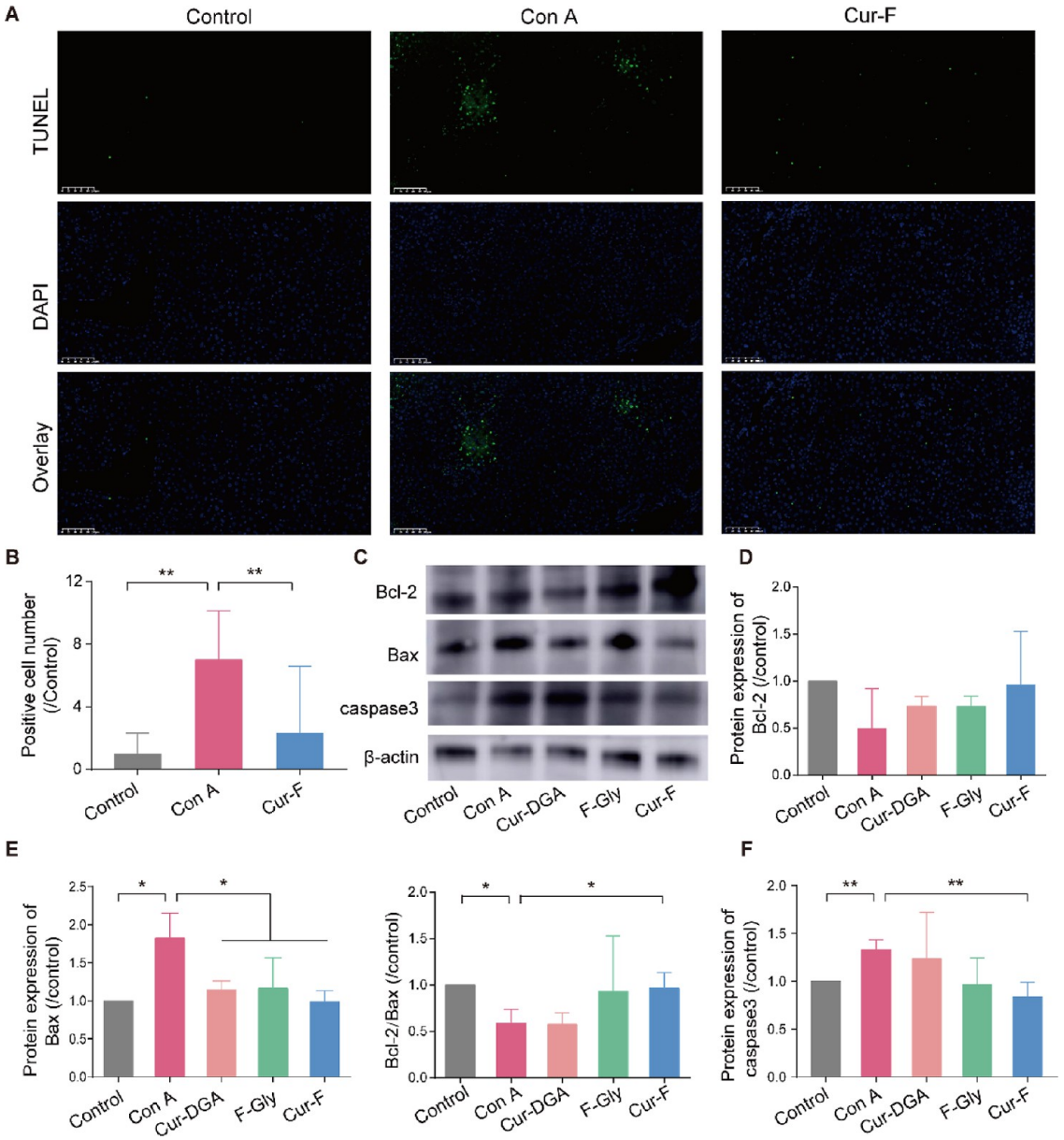

Figure 7. Cur-F suppresses hepatic apoptosis. (A) TUNEL staining of liver tissues. The scale bar is 100 μm. (B) Quantitative analysis of TUNEL staining. (C−F) WB and quantitative analyses of Bcl-2, Bax, and caspase3. Data are the mean ± SD n = 3−6 in each group. * represents $P < 0.05$ and ** represents $P < 0.01$, analyzed by ANOVA with LSD or Games−Howell tests.

of Cur-F. All these data depicted that Cur-F protected hepatocytes against apoptosis for alleviating AIH.

3.8. Biosafety of Cur-F. The biosafety of Cur-F was evaluated by H&E staining. The pathological analysis of the heart, lung, and kidneys showed that there were no obvious inflammatory infiltration and cellular necrosis after treatment by Cur-DGA, F-Gly, and Cur-F (Figure S14), exhibiting the neglectable adverse effects of Cur-F on major organs.

4. CONCLUSIONS

In summary, we successfully developed a curdlan-modified fullerene nanomaterial (Cur-F) for AIH therapeutics via reducing macrophage infiltration. Cur-F was prepared by the coupling reaction between amino groups on curdlan and carboxylic groups on fullerene carbon cages. It was demonstrated that Cur-F efficiently scavenged ROS and ameliorated oxidative stress in the liver of Con A-induced AIH mice. And Cur-F decreased the NF-κB signals, reduced the production of pro-inflammatory factors, and inhibited macrophage recruitment, alleviating hepatic inflammation. And thus, Cur-F reduced inflammation-induced hepatocyte apoptosis, exhibiting superior therapeutic effects for AIH with neglectable toxicity. This study provided a promising tactic for autoimmune diseases based on fullerenes.

■ ASSOCIATED CONTENT

Supporting Information

The Supporting Information is available free of charge at https://pubs.acs.org/doi/10.1021/acsami.3c16168.

^{1}H NMR, ^{13}C NMR, and ESI mass spectra of DGA-Boc; ^{1}H NMR, ^{13}C NMR, and ESI mass spectra of ALK-DGA-Boc; ^{1}H NMR, ^{13}C NMR, and ESI mass spectra of ALK-DGA; FT-IR spectroscopy and TGA of F-Gly; elemental analysis of F-Gly and Cur-F; hydrodynamic

https://doi.org/10.1021/acsami.3c16168
ACS Appl. Mater. Interfaces 2024, 16, 5536−5547

sizes of Cur-DGA and F-Gly; EPR of F-Gly; AFM image of Cur-F; liver index of mice after different treatments; TUNEL staining of liver tissues; H&E staining of the heart, lung, and kidneys; and the primers for Q-PCR (PDF)

AUTHOR INFORMATION

Corresponding Authors

Jingfen Han − *School of Chemistry and Chemical Engineering, Inner Mongolia University, Inner Mongolia 010021, China;* orcid.org/0000-0002-7295-0916; Email: hanjingfen@imu.edu.cn

Xue Li − *Key Laboratory of Molecular Nanostructure and Nanotechnology, Beijing National Laboratory for Molecular Sciences, Institute of Chemistry, Chinese Academy of Sciences, Beijing 100190, China; University of Chinese Academy of Sciences, Beijing 100049, China;* orcid.org/0000-0002-2289-3466; Email: lixue01@iccas.ac.cn

Authors

Chenglong Fei − *Key Laboratory of Molecular Nanostructure and Nanotechnology, Beijing National Laboratory for Molecular Sciences, Institute of Chemistry, Chinese Academy of Sciences, Beijing 100190, China; School of Chemistry and Chemical Engineering, Inner Mongolia University, Inner Mongolia 010021, China*

Lei Liu − *Key Laboratory of Molecular Nanostructure and Nanotechnology, Beijing National Laboratory for Molecular Sciences, Institute of Chemistry, Chinese Academy of Sciences, Beijing 100190, China; University of Chinese Academy of Sciences, Beijing 100049, China*

Hedong Qi − *Key Laboratory of Molecular Nanostructure and Nanotechnology, Beijing National Laboratory for Molecular Sciences, Institute of Chemistry, Chinese Academy of Sciences, Beijing 100190, China; University of Chinese Academy of Sciences, Beijing 100049, China*

Yuyang Peng − *Key Laboratory of Molecular Nanostructure and Nanotechnology, Beijing National Laboratory for Molecular Sciences, Institute of Chemistry, Chinese Academy of Sciences, Beijing 100190, China; University of Chinese Academy of Sciences, Beijing 100049, China*

Chunru Wang − *Key Laboratory of Molecular Nanostructure and Nanotechnology, Beijing National Laboratory for Molecular Sciences, Institute of Chemistry, Chinese Academy of Sciences, Beijing 100190, China; University of Chinese Academy of Sciences, Beijing 100049, China;* orcid.org/0000-0001-7984-6639

Complete contact information is available at: https://pubs.acs.org/10.1021/acsami.3c16168

Author Contributions

C.F. and L.L. contributed equally. Chenglong Fei: investigation, methodology, data curation, and formal analysis. Lei Liu: writing—original draft, data curation, and formal analysis. Hedong Qi: methodology and data curation. Yuyang Peng: data curation and visualization. Jingfen Han: conceptualization, writing—review and editing, and funding acquisition. Chunru Wang: supervision and funding acquisition. Xue Li: conceptualization, supervision, writing—review and editing, and funding acquisition.

Notes

The authors declare no competing financial interest.

ACKNOWLEDGMENTS

This work was supported by the Beijing Natural Science Foundation (2222090), the National Natural Science Foundation of China (52272048), the Inner Mongolia Education Department Fund Project (NJZY22722), and the Ministry of Science and Technology of China (2022YFA1205900). Dedicated to Prof. Chunli Bai on the occasion of his 70th birthday.

REFERENCES

(1) Heneghan, M. A.; Yeoman, A. D.; Verma, S.; Smith, A. D.; Longhi, M. S. Autoimmune hepatitis. *Lancet* **2013**, *382*, 1433−1444.

(2) Mieli-Vergani, G.; Vergani, D. Autoimmune hepatitis. *Nat. Rev. Gastroenterol. Hepatol.* **2011**, *8*, 320−329.

(3) Liwinski, T.; Schramm, C. Autoimmune hepatitis—update on clinical management in 2017. *Clin. Res. Hepatol. Gastroenterol.* **2017**, *41*, 617−625.

(4) Mieli-Vergani, G.; Vergani, D.; Czaja, A. J.; Manns, M. P.; Krawitt, E. L.; Vierling, J. M.; Lohse, A. W.; Montano-Loza, A. J. Autoimmune hepatitis. *Nat. Rev. Dis. Prim.* **2018**, *4*, 18017.

(5) Terziroli Beretta-Piccoli, B.; Mieli-Vergani, G.; Vergani, D. Autoimmmune hepatitis. *Cell. Mol. Immunol.* **2022**, *19*, 158−176.

(6) Montano Loza, A. J.; Czaja, A. J. Current therapy for autoimmune hepatitis. *Nat. Clin. Pract. Gastroenterol. Hepatol.* **2007**, *4*, 202−214.

(7) van den Brand, F. F.; van der Veen, K. S.; Lissenberg-Witte, B. I.; de Boer, Y. S.; van Hoek, B.; Drenth, J. P.; Verdonk, R. C.; Vrolijk, J. M.; van Nieuwkerk, C. M.; Bouma, G. Adverse events related to low dose corticosteroids in autoimmune hepatitis. *Aliment. Pharmacol. Ther.* **2019**, *50*, 1120−1126.

(8) Hoeroldt, B.; Mcfarlane, E.; Dube, A.; Basumani, P.; Karajeh, M.; Campbell, M. J.; Gleeson, D. Long-term Outcomes of Patients With Autoimmune Hepatitis Managed at a Nontransplant Center. *Gastroenterology* **2011**, *140*, 1980−1989.

(9) Webb, G.; Hirschfield, G.; Krawitt, E.; Gershwin, M. E. Cellular and molecular mechanisms of autoimmune hepatitis. *Annu. Rev. Pathol.: Mech. Dis.* **2018**, *13*, 247−292.

(10) Longhi, M. S.; Ma, Y.; Mieli-Vergani, G.; Vergani, D. Aetiopathogenesis of autoimmune hepatitis. *J. Autoimmun.* **2010**, *34*, 7−14.

(11) Lin, R.; Zhang, J.; Zhou, L.; Wang, B. Altered function of monocytes/macrophages in patients with autoimmune hepatitis. *Mol. Med. Rep.* **2016**, *13*, 3874−3880.

(12) Chen, T.-t.; Li, X.-q.; Li, N.; Xu, Y.-p.; Wang, Y.-h.; Wang, Z.-y.; Zhang, S.-n.; Qi, M.; Zhang, S.-h.; Wei, W.; et al. β-arrestin2 deficiency ameliorates S-100-induced autoimmune hepatitis in mice by inhibiting infiltration of monocyte-derived macrophage and attenuating hepatocyte apoptosis. *Acta Pharmacol. Sin.* **2023**, *44*, 2048−2064.

(13) Schümann, J.; Wolf, D.; Pahl, A.; Brune, K.; Papadopoulos, T.; van Rooijen, N.; Tiegs, G. Importance of Kupffer Cells for T-Cell-Dependent Liver Injury in Mice. *Am. J. Pathol.* **2000**, *157*, 1671−1683.

(14) Bosi, S.; Ros, T. D.; Spalluto, G.; Prato, M. Fullerene derivatives: an attractive tool for biological applications. *Eur. J. Med. Chem.* **2004**, *35*, 913−923.

(15) Yang, X.; Ebrahimi, A.; Li, J.; Cui, Q. Fullerene-biomolecule conjugates and their biomedicinal applications. *Int. J. Nanomed.* **2013**, *9*, 77−92.

(16) Li, X.; Zhen, M.; Zhou, C.; Yu, M.; Liu, L.; Shu, C.; Wang, C. Dual regulation on oxidative stress and endoplasmic reticulum stress by [70] fullerenes for reversing insulin resistance in diabetes. *Nano Today* **2022**, *45*, 101541.

(17) Li, X.; Zhen, M. M.; Yu, M. L.; Zhou, C.; Li, L.; Shu, C. Y.; Wang, C. R.; Bai, C. L. Gadofullerene nanoparticles extend survival rate and down-regulate thrombin expression in orthotopic pancreatic cancer. *Sci. China Mater.* **2022**, *65*, 508−517.

(18) Yin, J.-J.; Lao, F.; Fu, P. P.; Wamer, W. G.; Zhao, Y.; Wang, P. C.; Qiu, Y.; Sun, B.; Xing, G.; Dong, J.; et al. The scavenging of reactive oxygen species and the potential for cell protection by functionalized fullerene materials. *Biomaterials* **2009**, *30*, 611−621.
(19) Zhang, Y.; Shu, C.; Zhen, M.; Li, J.; Yu, T.; Jia, W.; Li, X.; Deng, R.; Zhou, Y.; Wang, C. A novel bone marrow targeted gadofullerene agent protect against oxidative injury in chemotherapy. *Sci. China Mater.* **2017**, *60*, 866−880.
(20) Yu, T.; Jia, W.; Zhen, M.; Zhou, Y.; Li, J.; Wang, C. Amino acid modified gadofullerene protects against insulin resistance induced by oxidative stress in 3T3-L1 adipocytes. *J. Mater. Chem. B* **2020**, *8*, 7521−7527.
(21) Ma, H.; Zhao, J.; Meng, H.; Hu, D.; Zhou, Y.; Zhang, X.; Wang, C.; Li, J.; Yuan, J.; Wei, Y. Carnosine-Modified Fullerene as a Highly Enhanced ROS Scavenger for Mitigating Acute Oxidative Stress. *ACS Appl. Mater. Interfaces* **2020**, *12*, 16104−16113.
(22) Liu, S.; Chen, D.; Li, X.; Guan, M.; Zhou, Y.; Li, L.; Jia, W.; Zhou, C.; Shu, C.; Wang, C.; et al. Fullerene nanoparticles: a promising candidate for the alleviation of silicosis-associated pulmonary inflammation. *Nanoscale* **2020**, *12*, 17470−17479.
(23) Dellinger, A.; Zhou, Z.; Lenk, R.; MacFarland, D.; Kepley, C. L. Fullerene nanomaterials inhibit phorbol myristate acetate-induced inflammation. *Exp. Dermatol.* **2009**, *18*, 1079−1081.
(24) Liao, X.; Zhao, Z.; Li, H.; Wu, B.; Huo, J.; Li, L.; Li, X.; Cao, X.; Xia, M.; Wang, C.; et al. Fullerene nanoparticles for the treatment of ulcerative colitis. *Sci. China: Life Sci.* **2022**, *65*, 1146−1156.
(25) Kuznietsova, H.; Lynchak, O.; Dziubenko, N.; Herheliuk, T.; Prylutskyy, Y.; Rybalchenko, V.; Ritter, U. Water-soluble pristine C60 fullerene attenuates acetaminophen-induced liver injury. *Bioimpacts* **2019**, *9*, 227−237.
(26) Gharbi, N.; Pressac, M.; Hadchouel, M.; Szwarc, H.; Wilson, S. R.; Moussa, F. [60] Fullerene is a powerful antioxidant in vivo with no acute or subacute toxicity. *Nano Lett.* **2005**, *5*, 2578−2585.
(27) Halenova, T.; Vareniuk, I.; Roslova, N.; Dzerzhynsky, M.; Savchuk, O.; Ostapchenko, L.; Prylutskyy, Y. I.; Ritter, U.; Scharff, P. Hepatoprotective effect of orally applied water-soluble pristine C 60 fullerene against CCl 4-induced acute liver injury in rats. *RSC Adv.* **2016**, *6*, 100046−100055.
(28) Li, X.; Zhen, M.; Zhou, C.; Deng, R.; Yu, T.; Wu, Y.; Shu, C.; Wang, C.; Bai, C. Gadofullerene Nanoparticles Reverse Dysfunctions of Pancreas and Improve Hepatic Insulin Resistance for Type 2 Diabetes Mellitus Treatment. *ACS Nano* **2019**, *13*, 8597−8608.
(29) Zhou, C.; Zhen, M.; Yu, M.; Li, X.; Yu, T.; Liu, J.; Jia, W.; Liu, S.; Li, L.; Li, J.; et al. Gadofullerene inhibits the degradation of apolipoprotein B100 and boosts triglyceride transport for reversing hepatic steatosis. *Sci. Adv.* **2020**, *6*, No. eabc1586.
(30) Lebre, F.; Hearnden, C. H.; Lavelle, E. C. Modulation of Immune Responses by Particulate Materials. *Adv. Mater.* **2016**, *28*, 5525−5541.
(31) Ryan, J. J.; Bateman, H. R.; Stover, A.; Gomez, G.; Norton, S. K.; Zhao, W.; Schwartz, L. B.; Lenk, R.; Kepley, C. L. Fullerene Nanomaterials Inhibit the Allergic Response. *J. Immunol.* **2007**, *179*, 665−672.
(32) Norton, S. K.; Wijesinghe, D. S.; Dellinger, A.; Sturgill, J.; Zhou, Z.; Barbour, S.; Chalfant, C.; Conrad, D. H.; Kepley, C. L. Epoxyeicosatrienoic acids are involved in the C70 fullerene derivative-induced control of allergic asthma. *J. Allergy Clin. Immunol.* **2012**, *130*, 761−769.e2.
(33) Zhang, R.; Edgar, K. J. Properties, chemistry, and applications of the bioactive polysaccharide Curdlan. *Biomacromolecules* **2014**, *15*, 1079−1096.
(34) Han, J.; Wang, X.; Liu, L.; Li, D.; Suyaola, S.; Wang, T.; Baigude, H. Click" chemistry mediated construction of cationic Curdlan nanocarriers for efficient gene delivery. *Carbohydr. Polym.* **2017**, *163*, 191−198.
(35) Wu, Y.; Cai, J.; Han, J.; Baigude, H. Cell Type-Specific Delivery of RNAi by Ligand-Functionalized Curdlan Nanoparticles: Balancing the Receptor Mediation and the Charge Motivation. *ACS Appl. Mater. Interfaces* **2015**, *7*, 21521−21528.
(36) Borjihan, G.; Zhong, G.; Baigude, H.; Nakashima, H.; Uryu, T. Synthesis and anti-HIV activity of −6-amino-6-deoxy-(1→3)-β-D-Curdlan sulfate. *Polym. Adv. Technol.* **2003**, *14*, 326−329.
(37) Rui, K.; Tian, J.; Tang, X.; Ma, J.; Xu, P.; Tian, X.; Wang, Y.; Xu, H.; Lu, L.; Wang, S. Curdlan blocks the immune suppression by myeloid-derived suppressor cells and reduces tumor burden. *Immunol. Res.* **2016**, *64*, 931−939.
(38) Brown, G. D.; Gordon, S. A new receptor for β-glucans. *Nature* **2001**, *413*, 36−37.
(39) Sun, Y.; Duan, B.; Chen, H.; Xu, X. A Novel Strategy for Treating Inflammatory Bowel Disease by Targeting Delivery of Methotrexate through Glucan Particles. *Adv. Healthcare Mater.* **2020**, *9*, 1901805.
(40) Ganbold, T.; Baigude, H. Design of Mannose-Functionalized Curdlan Nanoparticles for Macrophage-Targeted siRNA Delivery. *ACS Appl. Mater. Interfaces* **2018**, *10*, 14463−14474.
(41) Markovic, Z.; Trajkovic, V. Biomedical potential of the reactive oxygen species generation and quenching by fullerenes (C60). *Biomaterials* **2008**, *29*, 3561−3573.
(42) Guan, M.; Ge, J.; Wu, J.; Zhang, G.; Chen, D.; Zhang, W.; Zhang, Y.; Zou, T.; Zhen, M.; Wang, C.; et al. Fullerene/photosensitizer nanovesicles as highly efficient and clearable phototheranostics with enhanced tumor accumulation for cancer therapy. *Biomaterials* **2016**, *103*, 75−85.
(43) Huo, J.; Li, J.; Liu, Y.; Yang, L.; Cao, X.; Zhao, C.; Lu, Y.; Zhou, W.; Li, S.; Liu, J.; et al. Amphiphilic aminated derivatives of [60] fullerene as potent inhibitors of tumor growth and metastasis. *Adv. Sci.* **2022**, *9*, 2201541.
(44) Wang, H.-X.; Liu, M.; Weng, S.-Y.; Li, J.-J.; Xie, C.; He, H.-L.; Guan, W.; Yuan, Y.-S.; Gao, J. Immune mechanisms of Concanavalin A model of autoimmune hepatitis. *World J. Gastroenterol.* **2012**, *18*, 119.
(45) Yu, H.; Lin, L.; Zhang, Z.; Zhang, H.; Hu, H. Targeting NF-κB pathway for the therapy of diseases: mechanism and clinical study. *Signal Transduction Targeted Ther.* **2020**, *5*, 209.
(46) Van den Berg, R.; Haenen, G.; Van den Berg, H.; Bast, A. Transcription factor NF-κB as a potential biomarker for oxidative stress. *Br. J. Nutr.* **2001**, *86*, S121−S127.
(47) Lewis, S. M.; Williams, A.; Eisenbarth, S. C. Structure and function of the immune system in the spleen. *Sci. Immunol.* **2019**, *4*, No. eaau6085.
(48) Cano-Europa, E.; Blas-Valdivia, V.; Franco-Colin, M.; Gallardo-Casas, C. A.; Ortiz-Butrón, R. Methimazole-induced hypothyroidism causes cellular damage in the spleen, heart, liver, lung and kidney. *Acta Histochem.* **2011**, *113*, 1−5.
(49) Adams, J. M.; Cory, S. Bcl-2-regulated apoptosis: mechanism and therapeutic potential. *Curr. Opin. Immunol.* **2007**, *19*, 488−496.

https://doi.org/10.1021/acsami.3c16168
ACS Appl. Mater. Interfaces 2024, 16, 5536−5547